$Li_{24}[MnN_3]_3N_2$ and $Li_5[(Li_{1-x}Mn_x)N]_3$, Two Intermediates in the Decomposition Path of $Li_7[MnN_4]$ to $Li_2[(Li_{1-x}Mn_x)N]$: An Experimental and Theoretical Study

R. Niewa,* F. R. Wagner, W. Schnelle, O. Hochrein, and R. Kniep

Max-Planck-Institut für Chemische Physik fester Stoffe, Nöthnitzer Str. 40, D-01187 Dresden, Germany

Received April 17, 2001

The crystal structure of $Li_7[Mn^VN_4]$ was re-determined. Isolated tetrahedral $[Mn^VN_4]^{7-}$ ions are arranged with lithium cations to form a superstructure of the CaF_2 anti-type ($P\bar{4}3n$, No. 218, $a = 956.0(1)$ pm, $Z = 8$). According to measurements of the magnetic susceptibility, the manganese (tetrahedral coordination) is in a d^2 $S = 1$ state. Thermal treatment of $Li_7[Mn^VN_4]$ under argon in the presence of elemental lithium at various temperatures leads to $Li_{24}[Mn^{III}N_3]_3N_2$, $Li_5[(Li_{1-x}Mn_x)N]_3$, and $Li_2[(Li_{1-x}Mn^I_x)N]$, respectively. $Li_{24}[Mn^{III}N_3]_3N_2$ ($P\bar{3}1c$, No. 163, $a = 582.58(6)$ pm, $c = 1784.1(3)$ pm, $Z = 4/3$) crystallizes in a trigonal unit cell, containing slightly, but significantly nonplanar trigonal $[MnN_3]^{6-}$ units with C_{3v} symmetry. Measurements of the magnetic susceptibility reveal a d^4 $S = 1$ spin-state for the manganese (trigonal coordination). Nonrelativistic spin-polarized DFT calculations with different molecular models lead to the conclusion that restrictions in the Li−N substructure are responsible for the distortion from planarity of the $[Mn^{III}N_3]^{6-}$. $Li_5[(Li_{1-x}Mn_x)N]_3$ ($x = 0.59(1)$, $P\bar{6}2m$, No. 189, $a = 635.9(3)$ pm, $c = 381.7(2)$ pm, $Z = 1$) is an isotype of $Li_5[(Li_{1-x}Ni_x)N]_3$ with manganese in an average oxidation state of about +1.6. The crystal structure is a defect variant of the α-Li_3N structure type with the transition metal in linear coordination by nitrogen. $Li_2[(Li_{1-x}Mn^I_x)N]$ ($x = 0.67(1)$, $P6/mmm$, No. 191, $a = 371.25(4)$ pm, $c = 382.12(6)$ pm, $Z = 1$) crystallizes in the α-$Li_3N \hat{=} Li_2[LiN]$ structure with partial substitution of the linearly nitrogen-coordinated Li-species by manganese(I). Measurements of the magnetic susceptibility are consistent with manganese (linear coordination) in a low-spin d^6 $S = 1$ state.

Introduction

Nitrido-compounds of lithium with transition metals were first investigated by Juza et al.[1] For M = Co, Ni, Cu, the formation of substitution phases $Li_2[(Li_{1-x}M^I_x)N]$ was reported,[2] where M^I species substitute the linearly nitrogen-coordinated Li-site of the α-Li_3N[3] $\hat{=}$ $Li_2[LiN]$ crystal structure. Direct reactions of Li_3N with Fe or Mn under molecular nitrogen do not lead to the respective phases, but to compounds with higher oxidation states of the transition metal: $Li_3[Fe^{III}N_2]$,[4] $(Li_{1-x}Mn_{1+x})N$[5] and $Li_7[Mn^VN_4]$.[6] $Li_3[Fe^{III}N_2]$ and $Li_7[Mn^VN_4]$ have been shown to serve as precursors in reduction/decomposition reactions to obtain $Li_2[(Li_{1-x}M^I_x)N]$ phases of iron and manganese,[7] but little is known about these processes in detail. For the reduction of $Li_7[Mn^VN_4]$ to $Li_2[(Li_{1-x}Mn^I_x)N]$[8] under argon in the presence of lithium, we have identified two intermediates: $Li_{24}[Mn^{III}N_3]_3N_2$ and $Li_5[(Li_{1-x}Mn_x)N]_3$. In this work, we present the crystal structures of the precursor (a re-determination) and the different products obtained during the reaction. Furthermore, we compare the reaction in the presence of elemental lithium with the decomposition process in absence of alkali metal.

Experimental Section

Syntheses and Characterization. All manipulations were carried out under dry argon in a glovebox ($p(O_2, H_2O) < 0.1$ ppm). The reactions were carried out in tantalum crucibles contained within steel tubes. This assembly was placed in a quartz tube with back-pressure of the respective gas. Li_3N was prepared from elemental lithium (rods, Alfa, 99.9%) and nitrogen (Messer-Griesheim, 99.999%, additionally purified by passing over molsieve, Roth 3 Å, and BTS-catalyst, Merck) of ambient pressure at 673 K. Single-phase samples of $Li_7[Mn^VN_4]$ can be obtained from Li_3N, manganese powder (Chempur, 99.95%) and nitrogen of ambient pressure at temperatures between 973 and 1073 K. Single crystals were obtained from reactions of Li and Mn with nitrogen gas in the presence of Ba at 1073 K, besides the byproducts Li_3N and $Ba_3[MnN_3]$.[9] Microprobe analyses revealed no Ba presence in the crystals of $Li_7[Mn^VN_4]$. For preparation of the reduced nitridomanganates, $Li_7[Mn^VN_4]$ powder was heated to various temperatures under argon (Messer-Griesheim, 99.999%, additionally purified as described for N_2) in the presence of elemental lithium (typical molar ratio 1:10). After heat treatments with maximum temperatures $T_{max} \leq$ 1103 K, the X-ray diffraction powder pattern of $Li_7[Mn^VN_4]$ remained unchanged. In the range of 1103 K $\leq T_{max} \leq$ 1113 K $Li_{24}[Mn^{III}N_3]_3N_2$ was observed as well as $Li_7[Mn^VN_4]$ or $Li_5[(Li_{1-x}Mn_x)N]_3$. A single phase sample of $Li_{24}[Mn^{III}N_3]_3N_2$ (according to X-ray powder diffraction) was obtained from a mixture of $Li_7[Mn^VN_4]$ with lithium in a molar ratio of 1:2, which was heated under argon to 523 K within 2 h, held at this temperature for 10 h, then heated to 1103 K within 2.5 h and directly cooled to room temperature within 2 h. The product consisted of black single crystals and dark gray powder. Elemental analyses (hot-extraction technique on a LECO analyzer TC-463 DR) resulted in 29.4(8) % N ($Li_{24}[Mn^{III}N_3]_3N_2$ calcd: 31.7%) and 0.39(7) % O. (Even the smallest possible ordered occupation of a nonmetal site with oxygen instead of nitrogen, i.e., $Li_{24}[Mn^{III}N_3]_3N_{1.5}O_{0.5}$, would

* To whom correspondence should be sent. Fax: +49-351-4646-3002. E-mail: Niewa@cpfs.mpg.de.

(1) Juza, R.; Langer, K.; von Benda, K. *Angew. Chem.* **1968**, *80*, 373.
(2) Sachsze, W.; Juza, R. *Z. Anorg. Allg. Chem.* **1949,** *259*, 278.
(3) Zintl, E.; Brauer, G. *Z. Elektrochem.* **1935**, *41*, 102. Rabenau, A.; Schulz, H. *J. Less-Common Met.* **1976,** *50*, 155.
(4) Gudat, A.; Kniep, R.; Rabenau, A.; Bronger, W.; Ruschewitz, U. *J. Less-Common Met.* **1990**, *161*, 31.
(5) Niewa, R.; DiSalvo, F. J.; Yang, D.-K.; Zax, D. B.; Luo, H.; Yelon, W. B. *J. Alloys Compd.* **1998,** *266*, 32.
(6) Juza, R.; Anschütz, E.; Puff, H. *Angew. Chem.* **1959**, *71*, 161.
(7) Klatyk, J. PhD-Thesis, TU-Darmstadt, Germany 2000.
(8) Klatyk, J.; Kniep, R. *Z. Kristallogr. NCS* **1999**, *214*, 445.
(9) Tennstedt, A.; Röhr, C.; Kniep, R. *Z. Naturforsch.* **1993**, *48b*, 794.

10.1021/ic010412o CCC: $20.00
Published on Web 08/28/2001

Table 1. Crystallographic and Refinement Data

		$Li_7[MnN_4]$	$Li_{24}[MnN_3]_3N_2$	$Li_5[(Li_{1-x}Mn_x)N]_3$ $x = 0.59(1)$	$Li_2[(Li_{1-x}Mn_x)N]$ $x = 0.67(1)$
unit cell parameters	*a*, pm	956.0(1)	582.58(6)	635.9(3)	371.25(4)
	c, pm		1784.1(3)	381.7(2)	382.12(6)
V, 10^6 pm^3		873.8	524.4	133.7	45.2
Z		8	4/3	1	1
fw, g/mol		159.56	485.49	182.51	66.99
space group		$P\bar{4}3n$, No. 218	$P\bar{3}1c$, No. 163	$P\bar{6}2m$, No. 189	$P6/mmm$, No. 191
T, K		293	293	293	293
radiation λ, pm		71.073	71.073	71.073	71.073
density φ_{calcd}, g/cm^3		2.426	2.032	2.267	2.438
μ(Mo Kα), mm^{-1}		2.85	2.35	4.05	4.49
$R(F_o)^a$		0.0225	0.0143	0.0487	0.0206
R_w(all data)		0.0572	0.0346	0.1008	0.0566

[a] $R = \sum||F_o| - |F_c||/\sum|F_o|$ with $(F_o2 \geq 2\sigma(F_o2))$. [b] $R_w = [\sum w(|F_o2| - |F_c2)^2/\sum w|F_o2|^2]^{1/2}$.

calculate to at least 1.6% oxygen). Use of a slower heating rate or a higher maximum temperature of about 1123 K led to mixtures of $Li_{24}[Mn^{III}N_3]_3N_2$ and $Li_5[(Li_{1-x}Mn_x)N]_3$. Mixtures heated to a maximum temperature of 1173 K usually consisted of $Li_2[(Li_{1-x}Mn^{I}_x)N]$ as well as small amounts of $Li_{24}[Mn^{III}N_3]_3N_2$. A single phase sample of $Li_2[(Li_{1-x}Mn^{I}_x)N]$ was obtained at a maximum temperature of 1173 K and a dwelling time of 2 h at this temperature. Higher temperatures or longer dwelling times at 1173 K usually led to increasing amounts of binary manganese nitrides, ϵ-Mn_4N was observed frequently. Due to the small stability range, single phase samples of $Li_5[(Li_{1-x}Mn_x)N]_3$ could not be obtained so far.

For powder X-ray diffraction measurements, the samples were ground and sealed in glass capillaries (diameter 0.2 mm). The measurements were performed on a Huber image plate Guinier camera in the 2 Å-range of 10−100° (exposure time 1 h) using CuKα_1-radiation.

Crystal Structure Determinations. X-ray diffraction intensity data for a $Li_7[MnN_4]$ single crystal were collected on a Siemens P4 automatic four-circle diffractometer with graphite-monochromatized MoKα radiation, using the $\omega/2\theta$ scan technique. Unit cell parameters were determined from automatic centering of 25 reflections ($10° < \theta < 15°$) and refined by least-squares methods. 1747 reflections were measured in the range $3.0° < \theta < 30.0°$; 305 reflections were unique ($R_{int} = 0.0361$), and 260 reflections were assumed as observed applying the condition $I > 2\sigma(I)$. A correction for absorption effects was applied using Ψ-scans. X-ray diffraction intensity data sets of all other single crystals were taken on a MSC−Rigaku CCD with MoKα-radiation (Φ-scan 360°, 60° ω-scan at $\chi = 90°$, 0.5° steps with 40 s exposures, detector distance: 35 mm, 2 Å-offset: 10°). For the crystal structure determination of $Li_{24}[MnN_3]_3N_2$ three crystals were investigated. Refinements of the atomic occupancies lead to the compositions $Li_{24}[MnN_3]_3N_{1.86(2)}$, $Li_{24}[MnN_3]_3N_{1.89(9)}$ and $Li_{24}[MnN_3]_3N_{2.07(9)}$ indicating an oxidation state of manganese in the range of 2.9−3.1. Since the elemental analyses resulted in no significant oxygen contents (that would lower the oxidation state of manganese, see above) and the measurements of the magnetic susceptibility (see below) are in principle consistent with Mn^{III}, in the following we will refer to $Li_{24}[MnN_3]_3N_2$. Here we report the data of the best crystal, that resulted in the refined composition $Li_{24}[MnN_3]_3N_{1.86(2)}$: 2453 reflections were measured in the range $2.3° < \theta < 27.5°$; 413 reflections were unique ($R_{int} = 0.0519$), and 349 reflections were assumed as observed applying the condition $I > 2\sigma(I)$. Two crystals of $Li_5[(Li_{1-x}Mn_x)N]_3$ were investigated resulting in $x = 0.62(1)$ and 0.59(1). The crystallographic and refinement data for the latter are: 1337 reflections were measured in the range $3.7° < \theta < 27.6°$; 128 reflections were unique ($R_{int} = 0.0385$) of which all were assumed as observed applying the condition $I > 2\sigma(I)$. Unit cell parameters of several crystals of $Li_2[(Li_{1-x}Mn_x)N]$ were taken on the diffractometer. Earlier, a linear dependence of the unit cell parameters on *x* was observed.[7] According to these data, the unit cell parameters of all crystals determined in this study were consistent with $x \approx 0.67$. Intensity data were measured on two crystals leading to $x = 0.66(1)$ and 0.67(1). Data for one crystal with $x = 0.67(1)$ are: 341 reflections were measured in the range $5.3° < \theta < 26.1°$; 30 reflections were unique ($R_{int} = 0.0105$) of which all were assumed as observed applying the condition $I > 2\sigma(I)$. Absorption corrections based on symmetry-equivalent reflections were applied.[10] The crystal structures were solved and refined with the SHELX software packages.[11] Table 1 contains crystallographic and refinement data, positional and displacement parameters are given in the Tables 2−5.

Table 2. $Li_7[MnN_4]$. Selected Interatomic Distances (pm) and Angles (deg) (standard deviations in parentheses)

Mn(1)−	N(1)	4*x*	181.0(4)	N−Mn(1)−N	6*x*	109.47
Mn(2)−	N(2)	4*x*	182.6(3)			
Li(1)−	N(1)	2*x*	208.6(5)	N−Mn(2)−N	4*x*	108.35(6)
	N(2)	2*x*	216.4(5)		2*x*	111.7(1)
Li(2)−	N(2)	4*x*	212.2(2)			
Li(3)−	N(2)	4*x*	203.7(2)	Li(5)−N(2)		204.2(6)
				N(2)		209.6(5)
Li(4)−	N(1)		205.0(8)	N(2)		215.4(6)
	N(2)	3*x*	222.0(3)	N(1)		219.2(6)

Table 3. $Li_{24}[MnN_3]_3N_2$ Selected Interatomic Distances (pm) and Angles (deg) (standard deviations in parentheses)

Mn−N(1)	3*x*	178.4(1)		Li(3)−	N(2)		208.9(4)
					N(1)	3*x*	224.9(2)
Li(1)−N(1)		203.3(3)					
N(1)		213.3(2)		Li(4)−	N(1)	3*x*	206.8(1)
N(1)		218.2(2)			N(3)		240.6(4)
N(1)		226.2(3)					
Li(2)−N(2)		201.1(3)	∅	N(1)−	Li	(7*x*)	215
N(1)		212.8(2)	∅	N(2)−	Li	(8*x*)	203
N(3)		217.6(3)	∅	N(3)−	Li	(8*x*)	223
N(1)−Mn−N(1)	3*x*	117.55(2)					

Table 4. $Li_5[(Li_{1-x}Mn_x)N]_3$ ($x = 0.59(1)$). Selected Interatomic Distances (pm) and Angles (deg) (standard deviations in parentheses)

Mn/Li(1)−	N	2*x*	190.90(5)	N−Mn/Li(1)−N		177.3(5)
Li(2)−	N	2*x*	204(1)	N−Li(2)−N		146(2)
	N		239(4)		2*x*	107(1)
Li(3)−	N	3*x*	205.7(4)	N−Li(3)−N	3*x*	120

Table 5. $Li_2[(Li_{1-x}Mn_x)N]$ ($x = 0.67(1)$). Selected Interatomic Distances (pm) and Angles (deg) (standard deviations in parentheses)

Mn/Li(1)−	N	2*x*	191.05(5)	N−Mn/Li(1)−N		180
Li(2)−	N	3*x*	214.37(6)	N−Li(2)−N	3*x*	120

Magnetic Susceptibility Measurements. Measurements of the magnetization were done in a SQUID magnetometer (MPMS XL-7, Quantum Design) between 1.8 K−400 K at different magnetic fields (H_{ext} = 70 kOe, 35 kOe, 10 kOe, 1 kOe, 100 Oe, 40 Oe). Corrections for the sample containers were applied. Since the diamagnetic increment of N^{3-} is only poorly established, we did not correct for the core-diamagnetism. A typical field dependence of the molar magnetic susceptibility of the samples of $Li_{24}[Mn^{III}N_3]_3N_2$ and $Li_2[(Li_{1-x}Mn_x)N]$

(10) Jacobson, R. *Programm REQAB*, unpublished.
(11) Sheldrick, G.; Krüger, C.; Goddard, R. *SHELXS-86, Crystallographic Computing 3*′; Oxford University Press: New York, 1985. Sheldrick, G. *SHELXL97-2*; Göttingen, Germany, 1997.

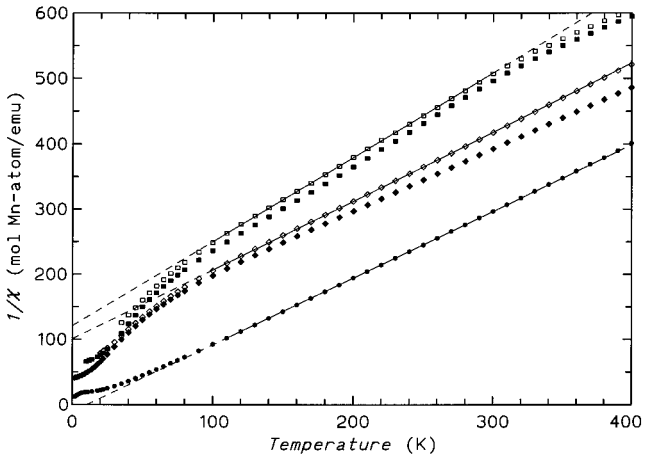

Figure 1. Magnetic susceptibility per Mn-atom of $Li_7[MnN_4]$ (35 kOe, full circles), $Li_{24}[MnN_3]_3N_2$ (70 kOe, full diamonds, and extrapolation to infinite field, open diamonds), and $Li_2[(Li_{1-x}Mn_x)N]$ ($x = 0.67$, 70 kOe, full squares and extrapolation to infinite field, open squares). The straight lines correspond to the fits of Curie−Weiss laws as given in Table 6.

($x = 0.67(1)$) can be explained by a minor impurity of a ferromagnetic or ferrimagnetic material with $T_C \gg 400$ K (probably ϵ-Mn_4N, T_C = 740 K);[12] therefore, extrapolations to infinite field were applied.

Theoretical. To explain the reason for the unusual nonplanar arrangement of the $[Mn^{III}N_3]^{6-}$ units found in the crystal structure of $Li_{24}[MnN_3]_3N_2$ (see below), nonrelativistic spin-polarized DFT (density functional theory) calculations on the GGA (generalized gradient approximation) level were carried out with the program system ADF2000[13] for spin triplet ($S = 1$) molecular units $[MnN_3Li_9]^{3+}$. The MOs were expanded in a large uncontracted set of Slater type orbitals containing diffuse functions. The basis sets (Slater-type basis functions) used for the three atom types correspond to the best basis sets available on standard (basis set type IV for Mn called "Mn.IV.2p"; basis set type V for Li and N called "Li.V", "N.V"): for Mn a triple-ζ basis set was used for 3d and 4s functions, augmented by one additional p-type polarization function. The stronger localized 3s and 3p states were described by a double-ζ basis and the energetically even lower lying 1s, 2s and 2p states were kept frozen (basis "Mn.IV.2p"). For the basis sets of Li and N, no frozen core approximation was applied. These consisted of a triple-ζ set for 2s and 2p states with one additional d and f polarization function. For the core 1s state, a double-ζ basis was used (basis "Li.V", "N.V"). An approximate density functional of the GGA-type was used throughout the calculations, which consists of the Becke's gradient corrections for the LDA (local density approximation) exchange part and the Lee−Yang−Parr correlation contribution (option "BLYP").[14]

Results

Magnetism. Figure 1 gives the temperature dependence of $1/\chi$ for $Li_7[Mn^VN_4]$, $Li_{24}[Mn^{III}N_3]_3N_2$, and $Li_2[(Li_{1-x}Mn_x)N]$ ($x = 0.67$). After correction of the molar susceptibility data, a Curie−Weiss law was fitted to the straight line portions of the plots. The resulting effective magnetic moments/Mn-atom μ_{eff} and Weiss constants Θ are listed in Table 6 together with the temperature range of data used for the fits, since all data deviate from the Curie−Weiss law for T below 100 K. Broad anomalies compatible with anti-ferromagnetic ordering of the phases are found. The temperatures $T_{ordering}$ are also indicated in Table 6.

Table 6. Parameters of Curie−Weiss Fits for the Magnetic Susceptibilities of $Li_7[MnN_4]$, $Li_{24}[MnN_3]_3N_2$, and $Li_2[(Li_{1-x}Mn_x)N]$ ($x = 0.67(1)$)

compound	temp range [K]	μ_{eff} [μ_B]	Θ [K]	$T_{ordering}$ [K]
$Li_7[MnN_4]$	110−390	2.79	+10.3	≈ 25/≈ 8
$Li_{24}[MnN_3]_3N_2$	100−400	2.75	−95	≈ 9
$Li_2[(Li_{1-x}Mn_x)N]$ ($x = 0.67(1)$)	100−300	2.5	−94	≈ 24

According to the magnetic susceptibility measurements on $Li_7[Mn^VN_4]$, the manganese (tetrahedral coordination) is in a d^2 $S = 1$ state ($\mu_{eff} = 2.79\ \mu_B$; spin-only: $\mu_{eff} = 2.83\ \mu_B$). Below 110 K, the data deviate from the Curie−Weiss behavior $\chi(T) = C/(T - \Theta)$; below about 8 K, weak ferromagnetic interactions occur, consistent with a positive $\Theta = 10.3$ K.

Above 100 K, the magnetic susceptibility of $Li_{24}[Mn^{III}N_3]_3N_2$ follows a Curie−Weiss expression $\chi(T) = C/(T - \Theta)$. We obtain $\Theta = -95$ K and an effective moment $\mu_{eff} = 2.75\ \mu_B$ per Mn-atom. For a Mn^{III} d^4 species, one would expect spin-only values of 4.90 μ_B for high-spin $S = 2$ and 2.83 μ_B for $S = 1$. Low-spin arrangements in nitridometalates(III) with trigonal planar units $[M^{III}N_3]^{6-}$ have previously been reported: $Ca_3[V^{III}N_3]$[15] d^2 was found in a low-spin state $S = 0$; $Ca_3[Cr^{III}N_3]$[16] d^3 is in a $S = {}^1/_2$ state at high temperatures, below 300 K it couples anti-ferromagnetically. Surprisingly, $(Ca_3N)_2[Mn^{III}N_3]$[17] d^4 was found to be diamagnetic suggesting a low-spin $S = 0$ state.

The data of the sample of $Li_2[(Li_{1-x}Mn_x)N]$ ($x = 0.67$) additionally show some curvature for $T > 300$ K. For 100 K < T < 300 K, we obtain $\Theta = -85$ K and an effective moment $\mu_{eff} = 2.5\ \mu_B$ per Mn-atom, consistent with a low-spin d^6 $S = 1$ Mn^I state of the manganese (linear coordination).

Crystal Structures. The $Li_7[Mn^VN_4]$ precursor contains isolated tetrahedra $[MnN_4]^{7-}$. The compound crystallizes in a distorted $2 \times 2 \times 2$ CaF_2 anti-type superstructure as earlier determined by Juza et al.[6] (Figure 2). Both the lithium and the manganese atoms occupy the fluorine site of the CaF_2 crystal structure in an ordered fashion. Nitrogen ligands of the tetrahedra $[MnN_4]^{7-}$ are located within a distorted cube formed from one manganese and seven lithium ions. $Li_7[Mn^VN_4]$ and $Li_7[P^VN_4]$[18] are isotypes. The crystal structures of $Li_7[Mn^VN_4]$ and the group 7 compounds $Li_7[M^VN_4]$ (M = V, Nb, Ta)[19−21] are closely related, but are no isotypes. The differences lie in the relative arrangements of the metal atoms within the cubic unit cell.[19] Distances d(Mn−N): 181.0(4) pm and 182.6(3) pm (Table 2) are close to those found for $Li_7[V^VN_4]$ (d(V−N): 181.3(6) pm and 185.1(3) pm).[19]

$Li_{24}[Mn^{III}N_3]_3N_2$ contains slightly nonplanar, trigonal $[MnN_3]^{6-}$ units and isolated nitride species exclusively coordinated by lithium ions within distorted cubes. These structural building units are stacked together with lithium to give a layered arrangement as depicted in Figure 3 (left). The trigonal $[MnN_3]^{6-}$ unit has C_{3v} symmetry; manganese is located about 28 pm out of the plane defined by the three coordinating nitrogen

(12) Wiener, G. W.; Berger, J. A. *J. Met.* **1955**, *7*, 360.
(13) *ADF Program System*, Release 2000.01, Scientific Computing and Modelling NV, Vrije Universiteit, Theoretical Chemistry, Amsterdam, The Netherlands. Baerends, E. J.; Ellis, D. E.; Ros, P. *Chem. Phys.* **1973**, *2*, 41. Versluis, L.; Ziegler, T. *J. Chem. Phys.* **1988**, *322*, 88. te Velde, G.; Baerends, E. J.; *J. Comput. Phys.* **1992**, *99(1)*, 84. Fonseca Guerra, C.; Snijders, J. G.; te Velde, G.; Baerends, E. J. *Theor. Chem. Acc.* **1998**, *99*, 391.
(14) Becke, A. D. *Phys. Rev. A* **1988**, *38*, 3098. Lee, C.; Yang, W.; Parr, R. G. *Phys. Rev. B* **1988**, *37*, 785. Johnson, B. G.; Gill, P. M. G.; Pople, J. A. *J. Chem. Phys.* **1993**, *98*, 5612. Russo, T. V.; Martin, R. L.; Hay, P. J. *J. Chem. Phys.* **1994**, *101*, 7729.
(15) Vennos, D. A.; DiSalvo, F. J. *J. Solid State Chem.* **1992**, *98*, 318.
(16) Vennos, D. A.; Badding, M. E.; DiSalvo, F. J. *Inorg. Chem.* **1990,** *29*, 4059.
(17) Gregory, D. H.; Barker, M. G.; Edwards, P. P.; Siddons, D. J. *Inorg. Chem.* **1995**, *34*, 5195.
(18) Schnick, W.; Lücke, J. *J. Solid State Chem.* **1990**, *87*, 101.
(19) Niewa, R.; Kniep, R. *Z. Kristallogr. NCS* **2001**, *216*, 5.
(20) Vennos, D. A.; DiSalvo, F. J. *Acta Crystallogr. C* **1992**, *48*, 610.
(21) Wachsmann, Ch.; Jacobs, H. *J. Alloys. Comput.* **1992**, *190*, 113.

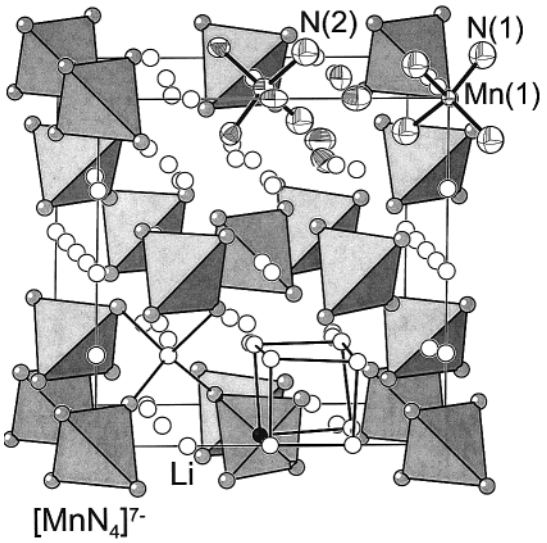

Figure 2. View of the unit cell of the crystal structure of $Li_7[MnN_4]$. Isolated tetrahedra $[MnN_4]^{7-}$ are stacked together with Li ions in an CaF_2 anti-type arrangement. Lithium ions are coordinated tetrahedrally by nitrogen, while the latter are surrounded by a distorted cube built of seven Li and one Mn. The unit cell of the crystal structure is indicated. Displacement ellipsoids in the top of the figure are drawn with 90% probability.

ligands. The distance d(Mn−N) = 178.4(1) pm (see Table 3) is close to those found for $[MnN_3]^{6-}$ ions with D_{3h} symmetry in $Sr_3[Mn^{III}N_3]$[9] (174.1(13) pm), $Ba_3[Mn^{III}N_3]$[9] (173.7(12) pm), and $(Ca_3N)_2[Mn^{III}N_3]$[17] (175.7(4) pm), and the $[MnN_3]^{6-}$ ion with C_{2v} symmetry in $Ca_3[Mn^{III}N_3]$[22] (1 × 179.9(5) pm, 2 × 179.4(4) pm). The second coordination shell around Mn^{III} is a distorted octahedron of lithium ions, which itself is a part of three neighboring edge-sharing cubes $MnLi_7$ surrounding the three nitrogen ligands of the trigonal $[MnN_3]^{6-}$ unit (compare Figure 4). The isolated nitrogen species occupy two distinct crystallographic sites; one is fully occupied, the other one refines to about one-third of full occupancy leading to compositions in the range of $Li_{24}[MnN_3]_3N_{1.9}$−$Li_{24}[MnN_3]_3N_{2.1}$ (compare crystal structure determination section). Both sites are surrounded by eight lithium ions forming distorted cubes. The fully occupied cube has shorter distances $\bar{d}$(N(2)−Li) = 203 pm than the partially occupied $\bar{d}$(N(3)−Li) = 223 pm, consistent with a higher Coulomb repulsion within the latter one. Similarly, the nitrogen ligands of the complex anions $[MnN_3]^{6-}$ are located in distorted cubes formed from seven Li and one Mn. Lithium is coordinated tetrahedrally (Li(1), Li(3), Li(4)) or trigonally (Li(2)) by nitrogen. Similar trigonal planar arrangements of lithium in nitrides were earlier observed in, e.g., $Li_2[LiN]$,[3] LiCaN[23] or $(Li_{1-x}Mn_{1+x})N$.[5] Additionally, considering one unoccupied central site in an elongated cube formed from two Mn and six Li, the compound can be written according to $Li_{32}[MnN_3]_4N_2(N_{1/3}\square_{2/3})_2\square_2$ (□ denotes a vacancy in the anionic sub-structure) and by this is described as a distorted CaF_2 anti-type superstructure variant with defects within the anionic nitride sub-structure. Thus, there are strong structural similarities to compounds such as $Li_{16}[NbN_4]_2O$,[24] $Li_{16}[TaN_4]_2O$,[25] $Li_{14}[CrN_4]_2O$[26] and $Li_{15}[CrN_4]_2N$,[26] which are all built from tetrahedra $[MN_4]^{x-}$ and isolated ions N^{3-} or O^{2-}, stacked together with Li^+ ions in various (defect) supercell arrangements of the CaF_2 anti-type structure. Figure 3 shows an exemplary comparison between the crystal structures of $Li_{24}[Mn^{III}N_3]_3N_2$ (left) and $Li_{14}[CrN_4]_2O$ (right). In the crystal structure of the nitridomanganate, the Li_8 cubes around isolated N^{3-} ions share common edges to form layers; in the nitridochromate the corresponding O-centered Li_8 cubes are not interconnected but isolated.

$Li_5[(Li_{1-x}Mn_x)N]_3$ (x = 0.59(1)) is an isotype of $Li_5[(Li_{1-x}Ni_x)N]_3$[27] and can be described as defect variant of the α-Li_3N structure $Li_5\square[(Li_{1-x}Mn_x)N]_3$. α-$Li_3N$ ≙ $Li_2[LiN]$ contains infinite chains $^1_\infty[LiN_{2/2}^{2-}]$ of alternating nitrogen and lithium atoms.[3] These chains are interconnected via further Li (in trigonal planar coordination) within the layers formed from the nitride species ("Li_2N"-layers). In the crystal structure of $Li_5[(Li_{1-x}Mn_x)N]_3$, the ordered defects of one-sixth of the lithium sites within the "Li_2N"-planes of the α-Li_3N crystal structure require a three times larger unit cell. The linearly by nitrogen coordinated site of the α-Li_3N crystal structure is partly substituted by Mn. Figure 5 compares these structures and Figure 6 gives the "Bärnighausen" symmetry tree[28] that leads from α-Li_3N (and $Li_2[(Li_{1-x}Mn_x)N]$) over Li[NiN][29] to $Li_5[(Li_{1-x}Mn_x)N]_3$. The oxidation state of manganese in $Li_5[(Li_{1-x}Mn_x)N]_3$ (x = 0.59(1)) calculates to about +1.6, similar to the results obtained for the isotypic Ni-phase (x = 0.63 ≙ $Ni^{+1.4}$; x = 0.77 ≙ $Ni^{+1.5}$).[7,27] $Li_2[(Li_{1-x}Mn^I_x)N]$ (x = 0.67(1)) crystallizes in the α-Li_3N structure with partial substitution of the linearly by nitrogen coordinated lithium species by manganese (compare Figures 5 and 6).

As observed earlier, the distances d((Li,M)-N) in both phase types $Li_5[(Li_{1-x}M_x)N]_3$ and $Li_2[(Li_{1-x}M_x)N]$ are shorter than the respective distance d(Li−N) obtained for α-Li_3N (α-Li_3N,[3] 193.8(1) pm; $Li_5[(Li_{0.23}Ni_{0.77}^{+1.4})N]_3$,[27] 179.0(5) pm; $Li_5[Ni^{+1.3}N]_3$,[29] 177.7(1) pm; Li[NiN],[29] 177.00(5); $Li_2[(Li_{0.37}Fe_{0.63}^I)N]$,[30] 181.5(1) pm; $Li_2[(Li_{0.57}Ni_{0.43}^I)N]$,[31] 183.8(1) pm). For M = Mn the deviation from the bond length in the crystal structure of α-Li_3N already was observed to be comparable small: $Li_2[(Li_{0.27}Mn_{0.73}^I)N]$,[8] 191.4(1) pm. This is in accordance with the distances d((Li,Mn)-N) in $Li_2[(Li_{0.33}Mn_{0.67}^I)N]$, 191.05-(5) pm and $Li_5[(Li_{0.41}Mn_{0.59}^{+1.6})N]_3$, 190.90(5) pm found in this study (compare Tables 4 and 5). Whether manganese in the latter compound should be addressed as mixed valent with distinct Mn^{1+} and Mn^{2+} species, or to be intermediate valent, as indicated by the occurrence of only one crystallographic site for Mn cannot be answered with the available data. Still, the shorter distance d((Li,Mn)-N) in $Li_5[(Li_{0.41}Mn_{0.59}^{+1.6})N]_3$ compared with $Li_2[(Li_{0.27}Mn_{0.73}^I)N]$ and $Li_2[(Li_{0.33}Mn_{0.67}^I)N]$, despite the lower Mn-contents on the respective site, already indicates a higher average oxidation state than +1.

Discussion

Direct reaction of Li_3N with manganese powder in the presence of molecular nitrogen leads to $Li_7[MnN_4]$ or $(Li_{1-x}Mn_{1+x})N$ ($0 \le x \le 0.33$, Mn oxidation state: 2−1.75),[5] depending on the ratio Li: Mn: n(Li)/n(Mn) ≥ 7 leads to the compound $Li_7[MnN_4]$, 7 > n(Li)/n(Mn) > 1 to a mixture of

(22) Tennstedt, A.; Röhr, C.; Kniep, R. *Z. Naturforsch*. **1993**, *48b*, 1831.
(23) Cordier, G.; Gudat, A.; Kniep, R.; Rabenau, A., *Angew. Chem*. **1989**, 101, 1689. *Angew. Chem., Int. Ed.* **1989**, 28, 1702.
(24) Wachsmann, Ch.; Jacobs, H. Z. *Kristallogr*. **1996,** *211*, 477. Chen, X. Z.; Eick, H. A. *J. Solid State Chem*. **1996**, *127*, 19.
(25) Wachsmann, Ch.; Brokamp, Th.; Jacobs, H. *J. Alloys Compd.* **1992**, *185*, 109.
(26) Gudat, A.; Haag, S.; Kniep, R.; Rabenau, A. *Z. Naturforsch*. **1990**, *45*, 111.
(27) Klatyk, J.; Höhn, P.; Kniep, R. *Z. Kristallogr*. **1998**, *213*, 31.
(28) Bärnighausen, H., *MATCH, Commun. Math. Chem*. **1980**, *9*, 139.
(29) Barker, M. G.; Blake, A. J.; Edwards, P. P.; Gregory, D. H.; Hamor, T. A.; Siddons, D. J.; Smith, S. E. *Chem. Commun*. **1999**, 1187.
(30) Klatyk, J.; Kniep, R. *Z. Kristallogr*. **1999**, *214*, 447.
(31) Gudat, A. Ph.D. Thesis. University of Düsseldorf, Germany, 1990.

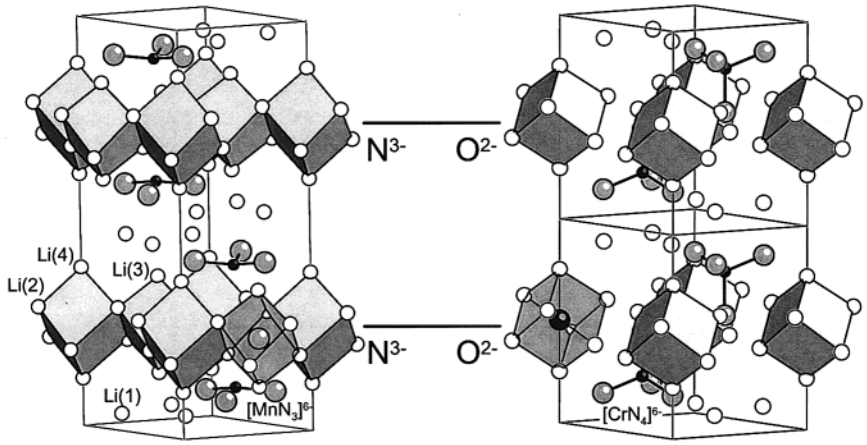

Figure 3. Comparison of the crystal structures of $Li_{24}[MnN_3]_3N_2$ (left, one unit cell) and $Li_{14}[CrN_4]_2O$[26] (right, 2 unit cells). The cubes are formed from eight lithium ions at the corners and are centered by one nitride (left) or oxide ion (right).

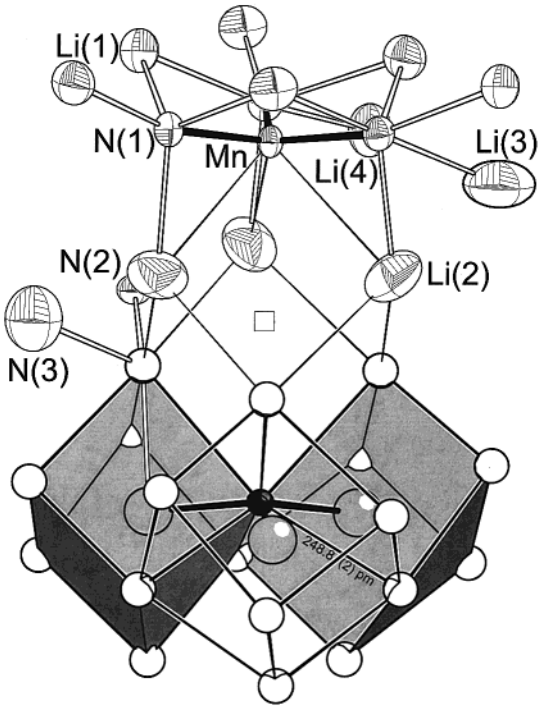

Figure 4. Section of the crystal structure of $Li_{24}[MnN_3]_3N_2$. The second coordination shell of Mn is a distorted octahedron of lithium ions (top), which itself belongs to edge-sharing cubes $MnLi_7$ surrounding the nitrogen species (bottom). The optimized molecular fragment $[MnN_3Li_9]^{3+}$ (see theoretical section) basically represents a part of the depicted crystal structure section (top). The trigonal coordination is indicated for one $Li(2)^+$ ion. The relation to a CaF_2 anti-type superstructure is given with an unoccupied site (denoted with □) in the center of an elongated Mn_2Li_6 cube. Note that shortest distances d(Li−Mn) = 248.8(2) pm occur to the opposite site of the plane defined by the three nitrogen ligands of the $[MnN_3]^{6-}$ trigonal ion. Displacement ellipsoids in the top of the figure are drawn with 90% probability.

$Li_7[MnN_4]$ and $(Li_{1-x}Mn_{1+x})N$, and $1 > n(Li)/n(Mn) > 0.5$ to the phase $(Li_{1-x}Mn_{1+x})N$. A nitridomanganate(I), $Li_2[(Li_{1-x}Mn^I_x)N]$ $0.73(2) \le x \le 0.77(2)$,[7,8] can be obtained by thermal decomposition of $Li_7[Mn^VN_4]$ in an argon atmosphere. Intermediates within this reaction/decomposition process were not characterized in previous studies. With the presented results, we are able to show that this reaction goes over at least two intermediates if lithium is added to the $Li_7[Mn^VN_4]$ precursor, and that the composition of the finally obtained substitution phase $Li_2[(Li_{1-x}Mn^I_x)N]$ depends on the reaction path.

Mixtures of $Li_7[Mn^VN_4]$ and elemental lithium showed no change in powder X-ray diffraction pattern or mass after heat treatments up to 1103 K in argon atmosphere. In a very small temperature window $Li_{24}[Mn^{III}N_3]_3N_2$ is formed, at higher temperatures $Li_5[(Li_{1-x}Mn_x)N]_3$ ($x \approx 0.60$, byproduct) and $Li_2[(Li_{1-x}Mn^I_x)N]$ ($x \approx 0.67$) are the reaction products. Hence, the reaction can be described as a stepwise reduction/decomposition from a manganese(V) compound, $Li_7[Mn^VN_4]$, over a nitridomanganate(III), $Li_{24}[Mn^{III}N_3]_3N_2$, to a phase with manganese in an average oxidation state between 1 and 2, $Li_5[(Li_{1-x}Mn_x)N]_3$ ($x \approx 0.60$, oxidation state of Mn +1.6), to finally yield the manganese(I) phase $Li_2[(Li_{1-x}Mn^I_x)N]$ ($x \approx 0.67$). A ternary intermediate lithium nitridomanganate(IV) corresponding to the recently reported $Li_6Ca_2[Mn_2^{IV}N_6]$[32] was not observed in this study. The precursor $Li_7[Mn^VN_4]$ and the first intermediate $Li_{24}[Mn^{III}N_3]_3N_2$ show strong similarities in their crystal structures, yet the former contains tetrahedra $[MnN_4]^{7-}$, while the latter contains trigonal, slightly nonplanar units $[MnN_3]^{6-}$ (see crystal structures section). Still, both can be described with CaF_2 superstructure variants, but in $Li_{24}[Mn^{III}N_3]_3N_2$ the Mn is moved from a tetrahedral hole in direction of a trigonal face. The structural changes from $Li_7[Mn^VN_4]$ to $Li_{24}[Mn^{III}N_3]_3N_2$ not only require the reduction of the Mn-center, but also complete rearrangement of all atoms under incorporation of lithium and release of nitrogen. Much closer is the crystallographic relation between $Li_5[(Li_{1-x}Mn_x)N]_3$ ($x = 0.59(1)$) and $Li_2[(Li_{1-x}Mn^I_x)N]$ ($x = 0.67(1)$). Under release of a comparably small amount of nitrogen (and simultaneous further reduction of Mn), the characteristic features of the crystal structure nearly remain unchanged. For both phases, the molar ratio $n(Li)/n(Mn) = 3.5$ was found to be constant within small limits, independent of the amount of elemental lithium added to the precursor. The earlier reported direct decomposition of $Li_7[Mn^VN_4]$ to $Li_2[(Li_{1-x}Mn^I_x)N]$ without elemental lithium in the initial reaction mixture yielded x in the range of 0.73(2) to 0.77(2) and, hence, in a noticeably lower ratio $2.9 \le n(Li)/n(Mn) \le 3.1$.[7,8] The latter fact is easily understood, since an intermediate with a higher ratio $n(Li)/n(Mn)$ than seven (as in $Li_{24}[Mn^{III}N_3]_3N_2$: $n(Li)/n(Mn) = 8$) is only possible with additional lithium in the reaction mixture if no byproducts are formed.

The small, but significant deviation of the $[MnN_3]^{6-}$ trigonal ion from planarity ($\Sigma\angle$(N−Mn−N) = 352.7°, Mn is situated d(Mn) = 28.2 pm above the plane defined by the three nitrogen

(32) Hochrein, O.; Grin, Yu.; Kniep, R. *Angew. Chem.* **1998**, *110*, 1667; *Angew. Chem., Int. Ed.* **1998**, *37*, 1582.

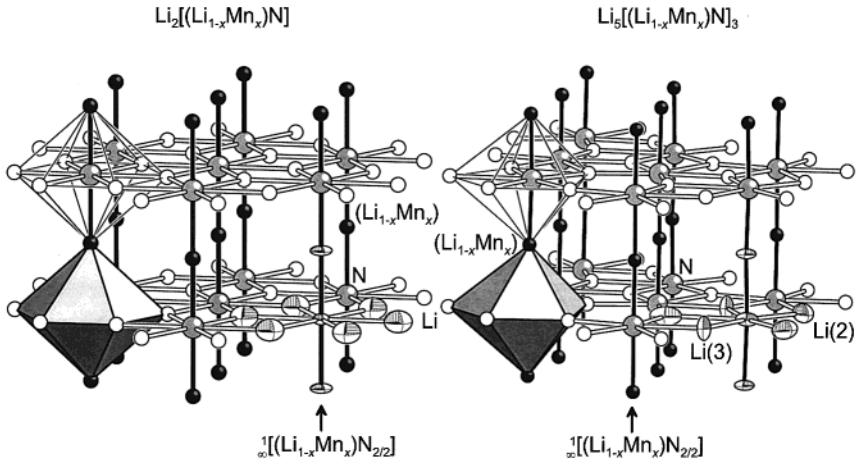

Figure 5. Comparison of the crystal structures of $Li_2[(Li_{1-x}Mn_x)N]$ ($x = 0.67(1)$, left) and $Li_5[(Li_{1-x}Mn_x)N]_3$ ($x = 0.59(1)$, right). In $Li_2[(Li_{1-x}Mn_x)N]$ the nitrogen species are coordinated by Mn_2Li_6 hexagonal bipyramids, in $Li_5[(Li_{1-x}Mn_x)N]_3$ ordered defects within the "Li_2N" layers of the former crystal structure lead to Mn_2Li_5 pentagonal bipyramids. Displacement ellipsoids are drawn with 50% probability.

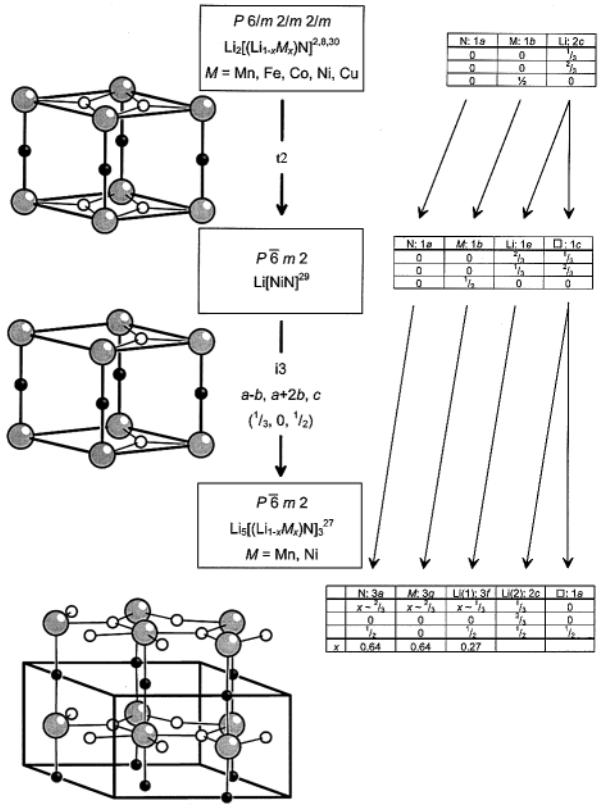

Figure 6. "*Bärnighausen*" symmetry tree[28] and relations between the crystal structures of $Li_2[(Li_{1-x}M_x)N]$[2,3,8,30] (M = Mn, Fe, Co, Ni, Cu) (top), Li[NiN][29] (middle) and $Li_5[(Li_{1-x}M_x)N]_3$ (M = Mn, Ni[27]) (bottom). Sites occupied with transition metal: black circles, nitrogen: gray circles, lithium: empty circles.

ligands) in $Li_{24}[Mn^{III}N_3]_3N_2$, hitherto unseen for nitridomanganates(III), led us to perform quantum chemical DFT-calculations. For trigonal planar ions $[MN_3]^{6-}$ with M = V, Cr, Fe ab initio calculations were already performed by Yee and Hughbanks[33] indicating that the chromium and the iron containing low spin species should display Jahn−Teller distortions (as observed experimentally for $Ca_3[CrN_3]$[16]), while an experimental observed distortion from D_{3h} to C_{2v} for the $[VN_3]^{6-}$ ion in $Ca_3[VN_3]$[15] appears to be due to the bonding of nitrogen to the coordinating alkaline earth ions. The bond analyses for $Ba_3[FeN_3]$ and $(Ca_3N)_2[FeN_3]$, both containing trigonal planar $[Fe^{III}N_3]^{6-}$ units with D_{3h} symmetry, indicated for the $3d_{z2}$ state above and below the iron species nonbonding behavior.[34,35] In the previously mentioned work, Yee and Hughbanks predict $[MnN_3]^{6-}$ to be a trigonal ion in a triplet $S = 1$ ground state as we observe for $Li_{24}[Mn^{III}N_3]_3N_2$. The distortion to C_{3v} of the $[MnN_3]^{6-}$ trigonal ion discussed here is not due to a first-order Jahn−Teller distortion since the 2-fold degenerate energy level does not split. The results of our calculations can be summarized as follows (see Tables 7−9):

Table 7. The Four Structures Used in the Pyramidalization Study of the $[MnN_3Li_9]^{3+}$ Unit as Part of the Crystal Structure of $Li_{24}[MnN_3]_3N_2$ are Given by the Following Z-matrix Scheme

	i	j	k	distance	angle	dihedral angle
XX						
Mn	1	0	0	1.00		
N	2	1	0	d(Mn−N)	∠(N−Mn-X)	
N	2	1	3	d(Mn−N)	∠(N−Mn-X)	120
N	2	1	3	d(Mn−N)	∠(N−Mn-X)	−120
Li	2	1	3	d(Li(2)−Mn)	∠(Li(2)−Mn-X)	60
Li	2	1	4	d(Li(2)−Mn)	∠(Li(2)−Mn-X)	60
Li	2	1	5	d(Li(2)−Mn)	∠(Li(2)−Mn-X)	60
Li	3	2	1	d(Li(1)−Mn)	∠(Li(1)−N-Mn)	180
Li	3	9	2	d(Li(1)−Mn)	∠(Li(1)−N-Li(1))	180
Li	4	2	1	d(Li(1)−Mn)	∠(Li(1)−N-Mn)	180
Li	4	11	2	d(Li(1)−Mn)	∠(Li(1)−N-Li(1))	180
Li	5	2	1	d(Li(1)−Mn)	∠(Li(1)−N-Mn)	180
Li	5	13	2	d(Li(1)−Mn)	∠(Li(1)−N-Li(1))	180

We performed series of geometry optimizations on idealized structural units $[MnN_3Li_9]^{3+}$ taken from the crystal structure. Structural idealizations concern (i) the local symmetry of the structural units, which is C_3 in the crystal (in contrast to the $[MnN_3]^{6-}$ ion with C_{3v} symmetry) and was set to C_{3v} in our models and (ii) the reduced number of Li atoms coordinating N. Efforts to use models with a lower positive charge (lower Li content) as, e.g., $[MnN_3Li_6]$, failed due to notorious problems with the spin density, which then was found on Li atoms and not on Mn.

We could find a structural model with bridging Li atoms, which is reliably close to the experimental structure and shows an energetic preference (total energy gain) for the pyramidalization (distortion from planarity due to Mn atom displacement)

(33) Yee, K. A.; Hughbanks, T. *Inorg. Chem.* **1992**, *31*, 1921.

(34) Stahl, D. Ph.D. Thesis. TU-Darmstadt, Germany 1994.

(35) Jansen, N.; Spiering, H.; Gütlich, P.; Stahl, D.; Kniep, R.; Eyert, V.; Kübler, J.; Schmidt, P. C. *Angew. Chem., Int. Ed. Engl.* **1992**, *104*, 1632; *31*, 1624.

Table 8. Values of Variables to Define the Four Structures Used in the Pyramidalization Study of the $[MnN_3Li_9]^{3+}$ Unit as Part of the Crystal Structure of $Li_{24}[MnN_3]_3N_2$[a]

variables	plan-Li_9N_3 d(Mn) = 0.0 optimized	plan-Li_9N_3 d(Mn) = 36.0 pm	pyr-Li_9N_3 d(Mn) = 0.0	pyr-Li_9N_3 d(Mn) = 36.0 pm optimized
d(Mn−N)	180.71 pm	184.26 pm	175.26 pm	178.92 pm
d(Li(2)−Mn)	240.27 pm	242.96 pm	221.75 pm	237.22 pm
d(Li(1)−N)	193.80 pm	193.80 pm	196.96 pm	196.96 pm
∠(N−Mn−X)	90° (fixed)	78.69°	90°	78.39°
∠(Li(2)−Mn−X)	90°	81.48°	68.67°	60.55°
∠(Li(1)−N−Mn)	117.43°	106.17°	97.33°	85.73°
∠(Li(1)−N−Li(1))	124.42°	124.42°	101.98°	101.98°

[a] The distance d(Li(1)−N) for both terminal Li atoms was kept equal during all optimizations. d(Mn) ≡ displacement of Mn from plane defined by the three N atoms. plan-Li_9N_3 ≡ fragment Li_9N_3 optimized with d(Mn) = 0.0 (fixed). pyr-Li_9N_3 ≡ fragment Li_9N_3 optimized with d(Mn) = 36.0 (optimized).

Table 9. Compilation of the Results of Three Pyramidalization Series of the $[MnN_3Li_9]^{3+}$ Unit as Part of the Crystal Structure of $Li_{24}[MnN_3]_3N_2$[a]

	d(Mn) = 0.0 pm	d(Mn) = 36.0 pm
	Planar Li_9N_3	
d(Mn−N)	180.7 pm	184.3 pm
d(Mn−Li^{bridge})	240.3 pm	243.0 pm
d(Mn−Li^{term})	320.1 pm	302.3 pm
d(N−Li^{bridge})	216.7 pm	216.7 pm
E(Pauli)	+20.3 eV	+18.4 eV
E(El.stat)	−21.5 eV	−20.6 eV
E(El.stat+corr.)	−22.2 eV	−21.3 eV
E(Orb.Int.)	−48.4 eV	−47.2 eV
$E_{tot} - E_{tot}$(minimum)	+0.25 eV	+0.35 eV
	Pyramidal Li_9N_3	
d(Mn−N)	175.3 pm	178.9 pm
d(Mn−Li^{bridge})	221.8 pm	237.2 pm
d(Mn−Li^{term})	279.9 pm	256.0 pm
d(N−Li^{bridge})	209.0 pm	209.0 pm
E(Pauli)	+25.4 eV	+22.8 eV
E(El.stat)	−21.3 eV	−20.3 eV
E(El.stat+corr.)	−21.8 eV	−21.1 eV
E(Orb. Int.)	−53.1 eV	−52.3 eV
$E_{tot} - E_{tot}$(minimum)	+0.87 eV	0.0

[a] The adiabatic pyramidalization (path 1, see text) from the planar to the pyramidal structure corresponds to the way from the top left to the lower right. Correspondingly, path 2a corresponds to the way from the lower left to the lower right, path 2b to the way from the top left to the top right. Energy contributions are given with respect to the fragments of spherical Mn^{3+} and Li_9N_3 in its respective structure. d(Mn) ≡ displacement of Mn from plane defined by the three N atoms. Plan-Li_9N_3 ≡ fragment Li_9N_3 optimized with d(Mn) = 0.0 (fixed). Pyr-Li_9N_3 ≡ fragment Li_9N_3 optimized with d(Mn) = 36.0 (optimized). E(Pauli) + E(El.stat+corr.) + E(Orb.Int.) = $E_{tot}^{fragments}$.

of the MnN_3 subunit. The local minimum structure, which was checked by a calculation of the harmonic vibration frequencies, exhibits a Mn displacement of 36.0 pm out of the plane defined by the N atoms compared to 28.2 pm obtained experimentally.

The local minimum structure for $[MnN_3Li_9]^{3+}$ (C_{3v} symmetry) with bridging Li atoms is a pyramidal one, which is more stable than the planar one (optimized, but forced to be planar) by ΔE_{tot}^{atoms}(pyr − plan)[36] = −0.7204 eV (−69.5 kJ/mol). The majority (66%) of the energy gain for the pyramidalization is due to the Li_9N_3 fragment: the total energy difference between both Li_9N_3 fragment structures is ΔE_{tot}^{atoms}(Li_9N_3, pyr − plan) = −0.4725 eV (−45.6 kJ/mol) leaving ΔE_{tot}^{atoms}(Mn−$N_3Li_9^{3+}$, pyr − plan) = −0.2479 eV (−23.9 kJ/mol) stabilization energy that are caused by interactions between the Mn atom and the Li_9N_3 fragment.

To further trace back the reason for the favorable interactions in the pyramidal structure, we performed a bonding energy analysis using an extended transition state method developed by Ziegler and Rauk,[37] which is implemented in the ADF2000[13] code. The bond energy is divided into basically three contributions: The Pauli repulsion energy, the electrostatic interaction energy and the orbital interactions energy. The first two terms, which are summarized in this terminology as steric interactions, were calculated from the combined fragments without optimizing the electronic degrees of freedom, i.e., before the scf (self-consistent field) cycle. The Pauli repulsion energy is caused by the unfavorable four-electron two-orbital interactions as, e.g., interactions between in-plane N(p_x, p_y) orbitals and occupied Mn($3d_{z2}$) orbitals or interactions between Li(1s) orbitals and occupied Mn(3s3p3d) orbitals. In general, it is mainly the Pauli repulsion that is responsible for keeping two fragments at their equilibrium distance.[37] In most cases, the electrostatic energy contribution is stabilizing and is caused by the interpenetration of the charge clouds of the two fragments beyond the respective screening effects. The overall small positive charge of the molecule used in our calculations additionally increased these favorable energy contributions. The stabilizing orbital interactions energy term was calculated after the scf cycle and is caused by polarization within each fragment and charge transfer between the fragments as a result of the optimized electronic degrees of freedom. This serves to relieve parts of the Pauli repulsion. In our example, it is the N(2p)-Mn($3d_{x2-y2}$, d_{xy})σ-bonding interaction built up from interactions of nitrogen lone pairs with empty Mn^{3+}($3d_{x2-y2}$, d_{xy}) orbitals which is mainly responsible for the stabilizing contributions. In the following, we analyze the energetics of the bond formation during pyramidalization in terms of the two separately converged fragments: a spherical Mn^{3+} ion and a Li_9N_3 molecule (in its respective structure), i.e., the bond energy is now almost completely determined by the interactions between Mn^{3+} and Li_9N_3. As a cross-check, we note that for this different choice of the fragments the stabilization energy for the pyramidalization $\Delta E_{tot}^{fragments}$($Mn^{3+}$-$N_3Li_9$, pyr − plan) = −0.2473 eV (−23.9 kJ/mol), which is within the accuracy needed for our discussion, is the same as ΔE_{tot}^{atoms}(Mn−N_3Li_93+, pyr − plan) = −0.2479 eV (−23.9 kJ/mol) for the atomic fragments.

We analyzed three different pyramidalization series for which the behavior of the different energy contributions can be

(36) The "atoms" superscript means that the bonding energy is calculated in comparison to spherical atomic fragments Mn, Li, N. As we are interested in bonding energy differences only, the reference system does not play a decisive role.

(37) Ziegler, T.; Rauk, A. *Theor. Chim. Acta (Berlin)* **1977**, *46*, 1−10. Ziegler, T. In *Metal−Ligand Interactions: from Atoms, to Clusters, to Surfaces*; Kluwer Academic Publishers: Norwell, MA, 1992; pp 367−396.

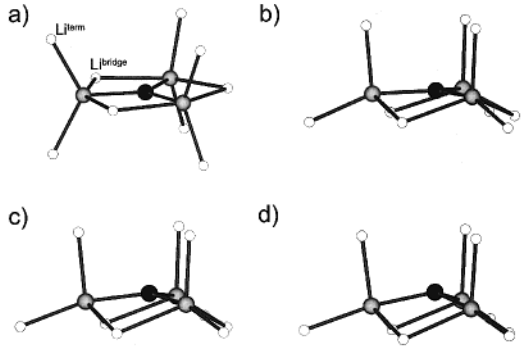

Figure 7. Structures for molecular units $[MnN_3Li_9]^{3+}$ as a part of the crystal structure of $Li_{24}[MnN_3]_3N_2$ used in the adiabatic pyramidalization path (manganese, black circles; nitrogen, gray circles; lithium, empty circles): (a) planar structure d(Mn) = 0.0 pm (fixed), unit optimized; (b) d(Mn) = 6.8 pm (fixed), unit optimized; (c) d(Mn) = 20.8 pm (fixed), unit optimized; (d) local minimum structure for d(Mn) = 36.0 pm (experimental 28.2 pm).

rationalized with the three distances d(Mn−N), d(Mn−Li^{bridge}), and d(Mn−Li^{term}) (see also Tables 7 and 8):

1.) The adiabatic pyramidalization: Starting from an optimized planar arrangement of Mn^{3+} and N atoms (if a coplanar arrangement of Mn and N atoms is enforced, the bridging Li atoms stay also within this plane, see Figure 7a), Mn^{3+} atoms were increasingly displaced out of the plane defined by the N^{3-} species and the Li_9N_3 fragment structure was allowed to adjust adiabatically. This means, we calculated a path of optimized geometries from the planar arrangement to the local minimum structure. A strong coupling between the Mn^{3+} displacement and the structure of the Li_9N_3 fragment could be observed (see Figure 7): as soon as the Mn atom was displaced from the coplanar arrangement with N and bridging Li atoms, the latter also moved out of the plane defined by N, but in the opposite direction. Simultaneously, the terminal Li atoms started to move into axial and equatorial positions. These structural changes in the Li_9N_3 fragment correspond to a rotation of the $NLi_2Li_{2/2}^{bridge}$ groups. Analyzing the bond energy contributions (compare Table 9) along the path from the energetically most unfavorable planar arrangement to the pyramidal local minimum structure, the energy is gained as a result of strongly increasing orbital interactions contributions which outweigh the increase of unfavorable steric interaction contributions. Latter increase is caused by simultaneous increase of destabilizing Pauli repulsion contributions and the decrease of stabilizing electrostatic interactions energy contributions. During the pyramidalization, it is mostly the strong decrease of the distance d(Mn−Li^{term}) which is mainly responsible for the increase of Pauli repulsion. At a displacement of Mn from the plane defined by the nitrogen species of d(Mn) = 36.0 pm (experimental: 28.2 pm), this repulsion reaches an equilibrium with the driving force for the pyramidalization, which is the decrease of the distance d(N−Li^{bridge}) under simultaneous avoidance of too strong Pauli repulsion with the Mn atom. As noted above, $\Delta E_{tot}^{fragments}$($Mn^{3+}$-$N_3Li_9$, pyr − plan) = −0.2473 eV (−23.9 kJ/mol).

2.a) The nonadiabatic pyramidalization, where the Li_9N_3 fragment structure was fixed to that of the local minimum: Mn^{3+} is displaced from a coplanar arrangement with the N atoms to the final local energy minimum displacement (36.0 pm). In contrast to the adiabatic path (1), the pyramidal structure now is not favored by the orbital interactions, which decrease on pyramidalization (increase of d(Mn−N)), but by the smallest (unfavorable) steric interactions (increase of d(Mn−Li^{bridge}) outweigh the decrease of d(Mn−$Li^{terminal}$)) which are dominated by the Pauli repulsion. The steric effects now were smaller than in the adiabatic path, because the Pauli repulsion and the electrostatic interactions show opposite behavior on the pyramidalization. Although the orbital interactions contributions are also smaller, the sum of all contributions, i.e., the energy gain along this path of pyramidalization, is $\Delta E_{tot}^{fragments}$($Mn^{3+}$-$N_3Li_9$, pyr − plan) = −0.8547 eV (−82.5 kJ/mol), which is more than 3 times larger than along the adiabatic path.

2.b) The nonadiabatic pyramidalization, where the Li_9N_3 fragment structure was fixed to that of the planar structure: Mn^{3+} atoms were displaced from a coplanar arrangement with the N atoms to the final displacement of 36.0 pm, which now corresponds to the most destabilized structure, demonstrating that the structure of the Li_9N_3 fragment plays the decisive role. Along this path, the Pauli repulsion contributions decrease on pyramidalization. This effect dominates the steric energy contributions; however, it is weakened by decreasing electrostatic energy contributions. The stabilizing orbital interactions contributions decrease on pyramidalization slightly stronger than the destabilizing steric effects decrease: the pyramidal structure is the energetically most unfavorable structure along this path. However, the potential curve for the displacement is very smooth: $\Delta E_{tot}^{fragments}$($Mn^{3+}$-$N_3Li_9$, pyr − plan) = 0.0971 eV (−9.4 kJ/mol).

As a summary, we can conclude that the observed pyramidalization is not a property contained within the $[Mn^{III}N_3]^{6-}$ unit, but is caused by the specific arrangement of Li coordinating N. The structural changes within the Li_9N_3 fragment, which are induced by the strong coupling with the Mn atom displacement, contribute 66% of the whole energy gain during the pyramidalization. In other words, the structural requirements of short distances d(Mn−N) and d(N−Li^{bridge}), long distances d(Mn−Li^{bridge}) and long distances d(Li−Li^{bridge}) are competing factors which cannot be satisfied simultaneously. The best solution to this dilemma turns out to be that with the pyramidal structure of the $[Mn^{III}N_3]^{6-}$ subunits. Finally, this explanation for the pyramidal structure of the $[Mn^{III}N_3]^{3-}$ subunits puts an alternative explanation of a slightly lower (average) oxidation state of the Mn species into the background (compare Experimental Section).

Acknowledgment. We thank U. Schmidt for performing the chemical analyses and H. Borrmann and R. Cardoso for collecting the X-ray diffraction data.

Supporting Information Available: Crystallographic data of $Li_7[MnN_4]$, $Li_{24}[MnN_3]_3N_2$, $Li_5[(Li_{1-x}Mn_x)N]_3$, and $Li_2[(Li_{1-x}Mn_x)N]$ in CIF format. This material is available free of charge via the Internet at http://pubs.acs.org.

IC010412O